

## Radiation Tolerant Nanowire Array Solar Cells

Pilar Espinet-Gonzalez, Enrique Barrigon, Gaute Otnes, Giuliano Vescovi, Colin Mann, Ryan M. France, Alex Justine Welch, Matthew Sullivan Hunt, Don Walker, Michael D Kelzenberg, Ingvar Åberg, Magnus T Borgström, Lars Samuelson, and Harry A Atwater

ACS Nano, **Just Accepted Manuscript** • DOI: 10.1021/acsnano.9b05213 • Publication Date (Web): 18 Oct 2019

Downloaded from [pubs.acs.org](https://pubs.acs.org) on October 22, 2019

### Just Accepted

“Just Accepted” manuscripts have been peer-reviewed and accepted for publication. They are posted online prior to technical editing, formatting for publication and author proofing. The American Chemical Society provides “Just Accepted” as a service to the research community to expedite the dissemination of scientific material as soon as possible after acceptance. “Just Accepted” manuscripts appear in full in PDF format accompanied by an HTML abstract. “Just Accepted” manuscripts have been fully peer reviewed, but should not be considered the official version of record. They are citable by the Digital Object Identifier (DOI®). “Just Accepted” is an optional service offered to authors. Therefore, the “Just Accepted” Web site may not include all articles that will be published in the journal. After a manuscript is technically edited and formatted, it will be removed from the “Just Accepted” Web site and published as an ASAP article. Note that technical editing may introduce minor changes to the manuscript text and/or graphics which could affect content, and all legal disclaimers and ethical guidelines that apply to the journal pertain. ACS cannot be held responsible for errors or consequences arising from the use of information contained in these “Just Accepted” manuscripts.

# Radiation Tolerant Nanowire Array Solar Cells

*Pilar Espinet-Gonzalez<sup>†</sup>, Enrique Barrigón<sup>‡</sup>, Gaute Otnes<sup>‡,#</sup>, Giuliano Vescovi<sup>§</sup>, Colin Mann<sup>¶</sup>,  
Ryan M. France<sup>⊥</sup>, Alex J. Welch<sup>†</sup>, Matthew S. Hunt<sup>∇</sup>, Don Walker<sup>¶</sup>, Michael D. Kelzenberg<sup>†</sup>,  
Ingvar Åberg<sup>§</sup>, Magnus T. Borgström<sup>‡</sup>, Lars Samuelson<sup>‡,§</sup> and Harry A. Atwater<sup>\*,†</sup>*

<sup>†</sup> Department of Applied Physics and Materials Science, California Institute of Technology,  
Pasadena, CA 91125, United States

<sup>‡</sup> Division of Solid State Physics, Lund University, Lund, SE-221 00, Sweden

<sup>§</sup> Sol Voltaics AB, Lund, SE-223 63, Sweden

<sup>¶</sup> The Aerospace Corporation, El Segundo, CA 90245-4609, United States

<sup>⊥</sup> National Renewable Energy Laboratory, Golden, CO 80401, United States

<sup>∇</sup> The Kavli Nanoscience Institute, California Institute of Technology, Pasadena, CA 91125,  
United States

<sup>#</sup> Institute for Energy Technology, Kjeller, NO-2007, Norway

\* e-mail: [haa@caltech.edu](mailto:haa@caltech.edu)

## ABSTRACT

Space power systems require photovoltaics that are lightweight, efficient, reliable, and capable of operating for years or decades in space environment. Current solar panels use planar multijunction, III-V based solar cells with very high efficiency, but their specific power (power to weight ratio) is limited by the added mass of radiation shielding (*e.g.* coverglass) required to protect the cells from the high-energy particle radiation that occurs in space. Here we demonstrate that III-V nanowire-array solar cells have dramatically superior radiation performance relative to planar solar cell designs and show this for multiple cell geometries and materials, including GaAs and InP. Nanowire cells exhibit damage thresholds ranging from ~10-40 times higher than planar control solar cells when subjected to irradiation by 100-350 keV protons and 1 MeV electrons. Using Monte Carlo simulations, we show that this improvement is due in part to a reduction in the displacement density within the wires arising from their nanoscale dimensions. Radiation tolerance, combined with the efficient optical absorption and the improving performance of nanowire photovoltaics, indicates that nanowire arrays could provide a pathway to realize high-specific-power, substrate-free, III-V space solar cells with substantially reduced shielding requirements. More broadly, the exceptional reduction in radiation damage suggests that nanowire architectures may be useful in improving the radiation tolerance of other electronic and optoelectronic devices.

## KEYWORDS

nanowire solar cells, radiation hard, space environment, space solar cells, high specific power, irradiation-induced defects, Monte Carlo simulations

1  
2  
3 Most spacecraft are powered by photovoltaic (PV) solar cells, which because of the challenging  
4 space environment are subject to stringent requirements, including high power conversion  
5 efficiency (PCE), high reliability, high tolerance to radiation, and high specific power, *i.e.* power-  
6 to-weight ratio. The latter requirement is crucial because the energy-generating system is typically  
7 one of the heaviest components of a satellite,<sup>1</sup> significantly impacting the cost of space launch.  
8 Thus substantial efforts have been made to increase the specific power of space solar panels, while  
9 ensuring that the solar cells will produce adequate power throughout the mission duration.  
10  
11  
12  
13  
14  
15  
16  
17  
18

19 In the space environment, solar panels are subject to severe thermal cycles, high UV light  
20 exposure, atomic oxygen in low earth orbit, space debris, meteoroid impact, electrostatic charging  
21 and high energy particle radiation. Standard space solar arrays composed of III-V solar cells  
22 degrade almost exclusively by high energy electron and proton irradiation. The radiation flux,  
23 energy distribution and fluence depend on the operating orbit, orientation of the spacecraft, solar  
24 cycle, and mission duration. Two main approaches are typically used to mitigate the detrimental  
25 effects of radiation. First, a layer of shielding (typically a cerium-doped cover glass) is used to  
26 reduce the amount of radiation reaching the solar cells, but this adds undesired weight.<sup>2</sup> The second  
27 approach to mitigate radiation damage is to increase the intrinsic radiation tolerance of the solar  
28 cells through choice of semiconductor materials and/or device architectures with enhanced  
29 radiation robustness, which experience less degradation for a given radiation exposure.<sup>3-7</sup>  
30  
31  
32  
33  
34  
35  
36  
37  
38  
39  
40  
41  
42  
43  
44

45 State-of-the-art space solar panels composed of III-V multijunction solar cells<sup>8,9</sup> are attractive  
46 because of high power conversion efficiencies (>30 % under extraterrestrial solar spectrum  
47 (AM0)), enabling a reduction in the panel area for a given mission. The development of thinned-  
48 substrate<sup>10</sup> and epitaxial lift-off (ELO)<sup>11</sup> technologies have allowed extremely thin III-V solar cells  
49 to be produced, such that the mass of the panels using these cells would be dominated largely by  
50  
51  
52  
53  
54  
55  
56  
57  
58  
59  
60

1  
2  
3 the requisite radiation-shielding. Yet, there is a growing demand for energy conversion systems  
4 with higher specific power than can be achieved with existing technologies (*i.e.*, exceeding  
5  $\sim 0.2$  W/g).<sup>12</sup> This demand is particularly driven by systems that need to operate in environments  
6 dominated by high proton fluence, such as medium earth orbit, which require heavy shielding  
7 because of the extensive exposure to radiation. Developing “rad-hard” thin-film solar cells would  
8 significantly reduce or even eliminate the need for shielding, thus maximizing the specific power.  
9

10  
11  
12 Many photovoltaic materials systems and cell geometries have been investigated for their  
13 potentially enhanced radiation tolerance. Studies have reported radiation-tolerant thin-film solar  
14 cells based on copper indium gallium diselenide (CIGS),<sup>13</sup> cadmium telluride (CdTe),<sup>14</sup> and, more  
15 recently, perovskite compounds.<sup>15-17</sup> In particular, perovskite solar cells have achieved impressive  
16 specific power values exceeding 29 W/g<sup>18</sup> and have demonstrated outstanding radiation resistance.  
17 While promising, these thin-film technologies are substantially less efficient and less  
18 technologically mature than state-of-the-art multijunction cells, and have not found widespread  
19 use in space. Within the established III-V compound semiconductor material systems, numerous  
20 approaches for radiation hardening have also been explored. Ultrathin (nanometer thickness),  
21 planar GaAs<sup>19</sup> has been demonstrated to reduce the short circuit current loss due to radiation  
22 damage, but thus far, such cells have demonstrated a low beginning-of-life (BOL) efficiency of  
23  $\sim 3$  %. Also, GaAs solar cells with quantum dots and quantum wells have been studied as potential  
24 candidates for radiation hard devices. Quantum dots and quantum wells have been reported to have  
25 enhanced radiation tolerance<sup>20,21</sup> owing to their reduced effective cross section for particle-solid  
26 interactions and carrier confinement. In solar cells, the current from the quantum dots and quantum  
27 wells is significantly radiation tolerant. However, the overall radiation behavior reported in highly  
28 performing optimized quantum dots/wells solar cells is similar to standard devices.<sup>7,22,23</sup>  
29  
30  
31  
32  
33  
34  
35  
36  
37  
38  
39  
40  
41  
42  
43  
44  
45  
46  
47  
48  
49  
50  
51  
52  
53  
54  
55  
56  
57  
58  
59  
60

1  
2  
3 Here we propose the use of III-V nanowire (NW) arrays as space solar cell architecture with  
4 dramatically enhanced radiation tolerance *versus* planar architectures. The NW solar cells consist  
5 of arrays of high-aspect-ratio semiconductor structures (“wires”) that have appropriate dimensions  
6 to enhance light absorption<sup>24-27</sup> and to reduce damage caused by high-energy particle radiation as  
7 we report here and it has been observed in photo-detectors.<sup>28-30</sup> The NW solar cells are fabricated  
8 from the same III-V phosphide and arsenide semiconductor compounds as conventional space  
9 solar cells. Although the NW technology is less mature, in principle, these cells should be capable  
10 of reaching similarly high efficiencies and reliability. Reported efficiencies of NW solar cells have  
11 been rapidly increasing over the last decade, yielding values of 15.3 % and 15.0 % (AM1.5G) for  
12 bottom up single-junction GaAs<sup>31</sup> and InP<sup>32</sup> NW solar cells respectively and 17.8 % for top down  
13 tapered dry-etched InP NW solar cells.<sup>33</sup> Furthermore, the NW growth processes can accommodate  
14 a far greater range of lattice mismatch than planar epitaxy, suggesting that defect-free  
15 multijunction cells could be grown from a diverse range of materials, to further improve the  
16 efficiency.<sup>34-38</sup> NW arrays have a low packing fraction (~9-14 %) and can be fabricated as devices  
17 in a substrate-free,<sup>39-41</sup> lightweight, flexible sheet form factor,<sup>42-45</sup> which is ideal for efficient  
18 packaging and deployment in space.  
19  
20  
21  
22  
23  
24  
25  
26  
27  
28  
29  
30  
31  
32  
33  
34  
35  
36  
37  
38  
39  
40  
41  
42

## 43 RESULTS AND DISCUSSION

44  
45 As high energy particles pass through a semiconductor crystal, they are slowed down by  
46 interactions with electrons and atomic nuclei, producing ionization and atomic displacements  
47 (vacancies and interstitial defects) in the crystal lattice that degrade material performance primarily  
48 by generation of nonradiative recombination centers. Particles with sufficient energy to completely  
49 penetrate the active region of the solar cell produce a roughly uniform damage concentration along  
50  
51  
52  
53  
54  
55  
56  
57  
58  
59  
60

1  
2  
3 their path.<sup>46</sup> However, particles with lower energies that come to rest inside the solar cell create an  
4 inhomogeneous defect distribution. In the case of electrons, the displacement rate  
5 (displacement/cm) decreases gradually as they are slowed down in the semiconductor. Protons  
6 exhibit the opposite behavior: as their energy decreases, the displacement rate increases  
7 dramatically, producing a highly non-uniform defect profile wherein most of the damage is  
8 concentrated near the end of the proton trajectory.<sup>46</sup> Shielding is primarily used to reduce the  
9 fluence of these highly damaging low-energy protons.<sup>46</sup> Therefore, any solar cell technology which  
10 aims to eliminate or to reduce drastically the shielding without compromising the service life of  
11 the solar array needs to be resistant not only to the radiation of high energy particles that penetrate  
12 the entire device, but also to lower-energy particles (mainly protons) with shorter penetration  
13 depth.

14  
15 To evaluate the radiation hardness of NW solar cells, we irradiated GaAs and InP NW solar cells  
16 with protons at energies of 100 keV and 350 keV, and electrons at 1 MeV energy. The initial  
17 efficiency under terrestrial spectrum (AM1.5G) for the GaAs NW solar cells was  $\sim 11.6 \% \pm 0.9 \%$   
18 and for the InP NW solar cells was  $\sim 6.5 \% \pm 0.9 \%$ . The GaAs NW cells had a wire length of  
19  $3\text{-}3.2 \mu\text{m}$ , whereas the InP NW cells had a wire length of  $1.7\text{-}2 \mu\text{m}$ . The GaAs NW cells had wire  
20 core radii of  $\sim 80 \text{ nm}$  and the InP NW cells of  $\sim 90 \text{ nm}$ . As experimental controls, we also included  
21  $4.4 \mu\text{m}$  thick ELO GaAs planar solar cells and  $\sim 1.3 \mu\text{m}$  thick InGaP cells. The cell geometries,  
22 representative cross sectional images and J-V curves before the irradiation tests are depicted in  
23 Figure 1. While the InP NW solar cells have moderate efficiencies, the performance of GaAs NW  
24 solar cells is comparable to that of the planar ELO GaAs solar cells. However, it should be noted  
25 that the planar devices do not have antireflective coatings; thus, a  $\sim 30 \%$  increase in current density  
26 could be expected for both the GaInP and GaAs planar cells if such a layer was used.

1  
2  
3  
4  
5 **Figure 1.** Schematics of all the devices tested (a-d), cross sectional images of representative NW  
6 solar cells (e-f) and initial J-V curves of representative devices of each architecture (1.g). Panel  
7 (1.e) shows a completed GaAs NW solar cell, which was overcoated with metal and ion-milled to  
8 enable cross-sectional imaging. Panel (1.f) shows as-grown InP NWs with the Au growth catalyst  
9 particle still on top of the wire. In (1.g), note that the planar cells lack antireflective coatings.  
10  
11  
12  
13  
14  
15  
16  
17  
18  
19

20 Performance degradation was evaluated in terms of the short circuit current density ( $J_{sc}$ ) and  
21 open circuit voltage ( $V_{oc}$ ), as shown in Figure 2. A summary of the devices included in each test,  
22 their initial characteristics and their performance after the irradiation is presented in Table S.1 in  
23 the Supplementary Information (SI).  
24  
25  
26  
27  
28  
29  
30

31 **Figure 2.** Solar cells performance after irradiation experiments. Degradation of the characteristic  
32 parameters ( $J_{sc}$  and  $V_{oc}$ ) of different solar cells architectures tested under irradiation with 100 keV  
33  $p^+$  (left panels), 350 keV  $p^+$  (center panels) and 1 MeV  $e^-$  (right panels). The points show the  
34 performance of the different solar cells included in each test. Data for the degradation of planar  
35 GaAs/Ge solar cells (red lines)<sup>47</sup> and for planar InP solar cells (green lines)<sup>4</sup> have been included  
36 for comparison.  
37  
38  
39  
40  
41  
42  
43  
44  
45  
46  
47

48 First, we analyzed the results of irradiation with 100 keV protons (left column panels in Figure  
49 2), which have a short penetration depth ( $\sim 750$  nm), such that the ions are implanted inside all of  
50 the tested devices. The degradation as a function of fluence (degradation rate) for both  $J_{sc}$  and  $V_{oc}$   
51 for our GaAs NW solar cells is lower than for the reference planar InGaP solar cell even though  
52  
53  
54  
55  
56  
57  
58  
59  
60



1  
2  
3 the InGaP is known to be a more radiation-tolerant material than GaAs.<sup>3</sup> Furthermore, the GaAs  
4  
5 NW degradation results are noticeably better than those previously reported for GaAs/Ge solar  
6  
7 cells.<sup>47</sup> The  $J_{sc}$  and  $V_{oc}$  of the GaAs NW solar cells follow the degradation slope of the GaAs/Ge  
8  
9 solar cell reported by Anspaugh but shifted to a fluence  $\sim \times 13$  times higher (see Figure S.1 in SI).  
10  
11 Regarding the InP NW solar cells, the remaining factor of the  $J_{sc} > 0.95$  after  $1 \cdot 10^{12} \text{ p}^+/\text{cm}^2$  is  
12  
13 notable in comparison with the degradation of standard space GaAs/Ge solar cells.<sup>47</sup> For InP NW  
14  
15 cells, the open circuit voltage degradation with irradiation is similar to that for GaAs NW solar  
16  
17 cells. However, due to the lower initial  $V_{oc}$  in the InP NW cells, the radiation resistance of the  $V_{oc}$   
18  
19 should be interpreted cautiously. Future improved InP NW structures with higher  $V_{oc}$  could have  
20  
21 a different radiation resistance.  
22  
23  
24  
25

26 We also analyzed results of cell irradiation with 350 keV protons (middle panels in Figure 2),  
27  
28 which have a penetration depth of  $\sim 2.4\text{-}2.9 \mu\text{m}$ . This is close to the full length ( $\sim 3\text{-}3.2 \mu\text{m}$ ) of the  
29  
30 GaAs NWs in our solar cells and we therefore would expect the protons to cause significant  
31  
32 damage therein as well as in the thin film GaAs planar ELO devices ( $\sim 4.4 \mu\text{m}$  thick). In the InP  
33  
34 NW solar cells ( $\sim 1.2\text{-}1.7 \mu\text{m}$  long), the protons cross the semiconductor structure. We found that  
35  
36 the GaAs NW solar cells can withstand a fluence  $\sim \times 40$  times higher than planar devices (see Figure  
37  
38 S.1 in SI). In particular, the short circuit current density degradation ratio ( $J_{sc}/J_{sc0}$ ), exceeds 0.90 at  
39  
40 the highest fluence  $1 \cdot 10^{12} \text{ p}^+/\text{cm}^2$  in the GaAs NW solar cells, which is comparable to that of InP  
41  
42 NW cells, and 9-fold times better than the short circuit current density degradation ratio in the  
43  
44 planar GaAs solar cells ( $J_{sc}/J_{sc0} \sim 0.1$ ), which are severely damaged. Likewise the degradation of  
45  
46  $V_{oc}$  in the GaAs NW solar cells ( $V_{oc}/V_{oc0} > 0.80$ ) is  $\times 1.8$  times lower than the planar thin film  
47  
48 GaAs solar cells tested.  
49  
50  
51  
52  
53  
54  
55  
56  
57  
58  
59  
60

1  
2  
3 Finally, we analyzed the results of irradiation with electrons of 1 MeV (right-hand panels in  
4 Figure 2), which penetrate around  $\sim 700 \mu\text{m}$  in the semiconductor, and consequently cross the  
5 entire solar cell in all devices. We found that the  $J_{\text{sc}}$  in the GaAs NW solar cells does not change  
6 when increasing the fluence up to  $1 \cdot 10^{15} \text{ e}^-/\text{cm}^2$  (equivalent to  $\sim 15$  years in geostationary orbit),  
7 and only decreases slightly ( $J_{\text{sc}}/J_{\text{sc}0} \sim 0.90\text{-}0.96$ ) after  $5 \cdot 10^{15} \text{ e}^-/\text{cm}^2$ , which indicates exceptional  
8 tolerance to electron irradiation<sup>3</sup> in comparison with previously reported data for various planar  
9 space GaAs solar cell architectures<sup>47,48</sup> where a short circuit current density degradation ratio  
10 ( $J_{\text{sc}}/J_{\text{sc}0}$ ) between 0.6-0.85 was observed at  $5 \cdot 10^{15} \text{ e}^-/\text{cm}^2$ . Also, the  $V_{\text{oc}}$  of the GaAs NW solar cells  
11 is unchanged at low and medium fluences. However, we observe an abrupt drop at the highest  
12 fluence, showing a similar degradation  $V_{\text{oc}}/V_{\text{oc}0}$  as seen in planar GaAs devices. Unlike the protons  
13 the 1 MeV electrons degradation curves of the planar and NW solar cells do not have the same  
14 shape which might indicate a different nature of the defects introduced in both architectures.<sup>49</sup> The  
15 InP NW solar cells also have lower degradation than previously reported values for different  
16 designs of planar InP solar cells<sup>4</sup> (green lines in the right-hand panels in Figure 2). A similar low  
17 short circuit current degradation rate has been reported for a planar InP solar cell with a very low-  
18 doped base. However, the  $V_{\text{oc}}$  degradation of the planar devices with a low doped base was  
19 significant  $V_{\text{oc}}/V_{\text{oc}0} = 0.81$ , in contrast to the InP NW-based devices where the degradation was  
20 almost negligible  $V_{\text{oc}}/V_{\text{oc}0} > 0.94$ . The initial  $V_{\text{oc}}$  of the InP NW solar cells is low (620-660 mV)  
21 so the radiation resistance advantage should be corroborated in more advanced devices with higher  
22 initial  $V_{\text{oc}}$ .

23  
24  
25  
26  
27  
28  
29  
30  
31  
32  
33  
34  
35  
36  
37  
38  
39  
40  
41  
42  
43  
44  
45  
46  
47  
48  
49  
50  
51  
52  
53  
54  
55  
56  
57  
58  
59  
60  
These results suggest that the surfaces of the NWs, particularly the interfaces between the InP  
NW core and the SiOx, as well as those for the GaAs core and  $\text{Al}_{0.9}\text{Ga}_{0.1}\text{As}$  shell, do not degrade  
significantly under irradiation by high energy particles under conditions known to degrade the

1  
2  
3 performance of cells.<sup>27,32,50</sup> NW solar cells made of different materials (InP, GaAs), with different  
4 architectures (*e.g.* junction geometry, wire length), and with different initial efficiencies ( $\sim 6.5\%$   
5 in InP NW cells and  $\sim 11.6\%$  in GaAs NW cells) have all demonstrated that both their  $V_{oc}$  and  $J_{sc}$   
6 are more resistant to radiation damage than their planar counterparts, for both proton and electron  
7 irradiation at various energies having different penetration depths in the semiconductor. It has been  
8 reported that cells made from lower-quality materials exhibit increased radiation tolerance,<sup>51</sup> thus  
9 since our NW cells have lower initial efficiencies than state-of-the-art planar cells, this may be  
10 partially responsible for their improved radiation tolerance. However, at least in the case of GaAs  
11 cells, our tests include both NW and planar devices with comparable and relatively high initial  $V_{oc}$   
12 ( $>0.9\text{ V}$ ), and in all conditions tested, the NW cells show a significantly higher radiation tolerance  
13 than planar devices. Therefore, collectively these results point to NW-based solar cells having  
14 superior radiation-tolerance compared to planar devices.  
15  
16  
17  
18  
19  
20  
21  
22  
23  
24  
25  
26  
27  
28  
29  
30  
31  
32

33 To understand the origin of the observed high radiation-tolerance of NW-based solar cells we  
34 performed Monte Carlo simulations<sup>52</sup> based on the binary collision approximation (BCA), which  
35 simulates the interaction of ions with matter by solving the classical scattering equation between  
36 the incoming ion and the target atom. We compared proton irradiation damage in a GaAs planar  
37 cell and in a GaAs NW array, using a simplified geometry consisting of a solid GaAs cuboid  
38  $1.5\ \mu\text{m}$  (width, X)  $\times$   $1.5\ \mu\text{m}$  (length, Y)  $\times$   $3.0\ \mu\text{m}$  (height, Z) for the planar solar cells, and for the  
39 NW array, an array of 9 GaAs NWs with a radius of 80 nm, a pitch of 500 nm and  $3\ \mu\text{m}$  long  
40 embedded in a cuboid with the same dimensions. Two sets of NW-structures (see Figure S.2 in SI)  
41 have been simulated, the first one consist of free-standing GaAs wires in vacuum (hereafter  
42  $NW_{\text{vacuum}}$ ), while in the second NW-structure, GaAs NWs are radially covered by an  $\text{Al}_{0.9}\text{Ga}_{0.1}\text{As}$   
43  
44  
45  
46  
47  
48  
49  
50  
51  
52  
53  
54  
55  
56  
57  
58  
59  
60

1  
2  
3 shell 30 nm wide, where the shell is enclosed with a 50 nm wide SiO<sub>2</sub> insulating layer and the NW  
4 array is in-filled with benzocyclobutene (BCB) making the array planar (NW<sub>core-shell</sub>). The core-  
5 shell planarized structure resembles the experimental GaAs NW solar cells tested, whereas the  
6 freestanding NWs are a notional structure. In the simulations, we irradiated the structures with a  
7 random distribution of protons (H<sup>+</sup>) at normal incidence to the top surface of each structure  
8 (perpendicular to the planar devices, parallel to the NW orientation for the NW-based devices).  
9 Periodic boundary conditions were assumed in all structures to reproduce an infinite array. The  
10 distributions of arsenic displacements (these are the primary defects reported on irradiated *n*- and  
11 *p*-type GaAs<sup>49</sup>) have been calculated. Further details on the simulation procedure are presented in  
12 the Methods section.  
13  
14  
15  
16  
17  
18  
19  
20  
21  
22  
23  
24  
25

26 The arsenic displacements produced per incident H<sup>+</sup> (damage) as a function of the ion energy  
27 are shown in Figure 3.a) for the planar architecture. The damage (#displacements/ion) introduced  
28 in the planar device increases with proton energy up to ~350 keV. At this energy, protons are  
29 implanted at the bottom of the GaAs (see Figures 4 and 5) after undergoing numerous collisions  
30 in the slowdown process. At higher energies, protons cross the entire semiconductor and  
31 consequently the interactions with the GaAs atoms are drastically reduced. Figure 3.b) illustrates  
32 the damage ratio of the planar architecture to the NW array (left axis). The results indicate that the  
33 damage in the planar structure is noticeably higher, whereas only a small part of the ion energy is  
34 deposited in the wires of the array. The benefit of the NW architecture is particularly advantageous  
35 at the energies which produce the most detrimental effects in the planar geometry. In all cases, the  
36 free-standing NW arrays (NW<sub>vacuum</sub>) exhibit the lowest damage.  
37  
38  
39  
40  
41  
42  
43  
44  
45  
46  
47  
48  
49  
50

51 Three effects can happen concurrently in the interaction of high energy protons with NW arrays:  
52 1) some of the ions that impinge on the space between wires can leave the array without depositing  
53  
54  
55  
56  
57  
58  
59  
60

1  
2  
3 their energy in the wires (particularly in free-standing NWs), 2) some of the ions that initially  
4 impinge on a wire or their secondary recoils can be scattered out of the wire and 3) some of the  
5 ions that initially enter the array through the infilled material or their secondary recoils can be  
6 deflected towards a wire. The array geometry, the density of the different materials used and their  
7 stopping power are the main parameters which determine the distribution of the irradiation induced  
8 defects in the different layers of the NW array. On the other hand, from the viewpoint of optical  
9 absorption, photons which impinge in the area between wires are absorbed because NWs have  
10 optical absorption cross sections which are greater than their physical cross sections. Therefore, in  
11 addition to a comparison of damage (#displacements/ion) integrated over the cuboid volume  
12 (1.5  $\mu\text{m}$  x 1.5  $\mu\text{m}$  x 3  $\mu\text{m}$ ) for the different architectures, the comparison of the damage introduced  
13 in the volume covered by GaAs has been included in Figure 3.b) (right axis). At all the energies  
14 and for both NW arrays (core-shell and vacuum) the ratio of As displacement/ion in planar *versus*  
15 NW architectures exceeds unity, confirming an effective drop in cross section for defect  
16 production in the NWs.  
17  
18  
19  
20  
21  
22  
23  
24  
25  
26  
27  
28  
29  
30  
31  
32  
33  
34  
35  
36  
37

38 **Figure 3.** Comparison of the damage introduced by protons of different energies in planar and NW  
39 solar cells. Figure 3.a) Arsenic displacements produced per incident ion in a planar architecture  
40 *versus* different proton energies. Figure 3.b) Damage ratio of the planar to the NW array (left axis)  
41 and damage ratio in GaAs of the planar to the NWs (right axis).  
42  
43  
44  
45  
46  
47  
48  
49

50 In order to have a better understanding of the damage features observed in Figure 3, the As  
51 displacement distributions obtained at 100 keV proton irradiation ( $\text{H}^+$  stop near the top surface),  
52 350 keV proton irradiation ( $\text{H}^+$  stop near the bottom surface) and 500 keV proton irradiation ( $\text{H}^+$   
53  
54  
55  
56  
57  
58  
59  
60

1  
2  
3 cross the semiconductor) are given in Figure 4. The induced damage per Angstrom has been  
4 integrated over the solar cell thickness (XY plane integrated over Z) in the top plots of Figure 4  
5 and over the array width (YZ plane integrated over X) in the bottom plots. The variation in the  
6 number of irradiation-induced defects in the different architectures is exhibited in the top plots. As  
7 shown in Figure 3.b), the damage in the planar architecture is always higher than in the NWs and  
8 particularly advantageous is the free-standing NW configuration ( $NW_{\text{vacuum}}$ ). The bottom plots in  
9 Figure 4 reveal that not only the number of irradiation-induced defects varies in the different device  
10 architectures but also their depth distribution within the cell.

11  
12 The penetration profiles of irradiation-induced damage per Angstrom averaged over the array  
13 area ( $1.5 \mu\text{m} \times 1.5 \mu\text{m}$ , @array) and over the NWs surface coverage ( $9 \times \pi \times (80 \text{ nm})^2$ , @NW) are  
14 represented in Figure 5 for a better visual comparison. In the NW solar cells, the particle tracks in  
15 the collision cascade are truncated radially at the surfaces of the NWs, thereby reducing or  
16 eliminating the characteristic peak of induced displacements relative to that observed in bulk  
17 materials. The ions and recoils that radially leave the NWs continue the slowdown process in the  
18 surrounding material, as observed in Figures S.3. In particular, 350 keV protons are significantly  
19 scattered in the planar structure and therefore the truncation of the collisions in the NW array is  
20 markedly pronounced. The advantage of the NW array is less significant at proton energies that  
21 create a moderate number of scattering events in a planar configuration. On the other hand, the  
22 scattering events in the surrounding photovoltaically inactive material can deflect high energy  
23 particles (ions or recoils) towards the NWs. In fact, for proton energies at which all the protons are  
24 implanted in the NW array (such as 100 keV) the damage originated in the NWs by scattered high  
25 energy particles coming from the surrounding material is not negligible. In Figure 5.a), two distinct  
26 regions in the irradiation-induced defect profile are observed, a first region ( $< 750 \text{ nm}$ ) where the  
27  
28  
29  
30  
31  
32  
33  
34  
35  
36  
37  
38  
39  
40  
41  
42  
43  
44  
45  
46  
47  
48  
49  
50  
51  
52  
53  
54  
55  
56  
57  
58  
59  
60

1  
2  
3 displacements predominantly originate *via* ions or recoils impinging on the NWs and a second  
4 region (>850 nm) deeper inside the wire where the displacements observed originate *via* collisions  
5 from scattered high energy particles that initially impacted on the surrounding material. However,  
6 as revealed in Figure 3.b), the overall damage introduced in the NWs is lower than in the planar  
7 configuration.

8  
9  
10  
11  
12  
13  
14  
15 Finally, the damage in the notional free-standing NW array simulated is even lower than in the  
16 core-shell planarized NW array. In the free-standing NWs the ions can move undisturbed between  
17 NWs favoring larger angular and lateral spreading and ultimately enabling ions to leave the array  
18 without depositing their energy. Also, the free movement of ions between wires produces a very  
19 different defect distribution with a peak-free damage curve dispersed along the whole wire length  
20 (see Figure 5).

21  
22  
23  
24  
25  
26  
27  
28  
29  
30  
31 **Figure 4.** Damage distribution per Angstrom in planar and NW solar cells after the irradiation  
32 with protons of different energies. Front view of the As displacement distribution per ion and  
33 Angstrom integrated over the solar cell thickness (Z) (top plots) and lateral view of the As  
34 displacement distribution per ion and Angstrom integrated over the solar cell width (X) (bottom  
35 plots) for different proton energies (100 keV, 350 keV and 500 keV) and solar cell's architectures.

36  
37  
38  
39  
40  
41  
42  
43  
44  
45 **Figure 5.** In-depth induced-damage per Angstrom in planar and NW solar cells for different proton  
46 energies. Arsenic displacements averaged over the whole array area (@array dotted lines) and over  
47 the nanowires area (@NW solid lines) for the different device architectures and representative  
48 proton energies.

1  
2  
3 The energy requirements for space power systems demand lightweight, efficient and radiation  
4 hard PV materials and devices designed for high specific power. In this study, we have assessed  
5 III-V NW solar cells for space applications by irradiation using high energy protons and electrons  
6 and by simulating the implications of their reduced dimensions in the generation of particle  
7 irradiation-induced defects.  
8  
9  
10  
11  
12  
13

14 Based on our experiments, we determined that the degradation of III-V NW solar cells is  
15 significantly lower than their planar III-V counterparts for both high energy protons with a short  
16 penetration depth (100 keV and 350 keV) and high energy electrons (1 MeV) which cross the  
17 entire solar cells. The high radiation tolerance exhibited by the NW solar cells implies that 1) NW  
18 solar cells require less (and potentially no) shielding against low energy protons and 2) NW solar  
19 cells can potentially extend the lifetime of the mission since the unshielded high energy particles  
20 with high penetration depth are also less harmful in NW solar cells.  
21  
22  
23  
24  
25  
26  
27  
28  
29

30 Since the planar and NW solar cells tested are compound of the same III-V semiconductor  
31 materials, the irradiation results suggest that the radiation hardness of NW solar cells benefit from  
32 their array geometry and nanometric dimensions. A Monte Carlo BCA model has been used to  
33 compare proton irradiation induced damage in a planar GaAs architecture and in a NW array  
34 resembling the device architecture of our irradiated experimental NW solar cells. The Monte Carlo  
35 BCA model reveals a lower damage in the NWs than in the planar solar cells across the entire  
36 proton energy spectrum. The reduction in the irradiation-induced defect density is mainly due to  
37 the truncation of collisions in the nanometer-scale wires. Monte Carlo simulations reproduce the  
38 trend observed experimentally that the NW array configuration is particularly advantageous at  
39 proton energies that induce a large number of scattering events in planar absorber structures. As a  
40 result, the benefit of the NW architecture is more pronounced for irradiation with 350 keV protons  
41  
42  
43  
44  
45  
46  
47  
48  
49  
50  
51  
52  
53  
54  
55  
56  
57  
58  
59  
60



1  
2  
3 than with 100 keV protons. However, the radiation hardness observed experimentally is higher  
4  
5 than the Monte Carlo BCA simulations predict. In fact, the damage ratio of the planar to the NW  
6  
7 architecture estimated by the Monte Carlo simulations is approximately ten-fold lower than the  
8  
9 radiation hardness observed experimentally in the irradiation tests. Monte Carlo BCA simulations  
10  
11 model ballistic collisions of the incident ion and the generated recoils on a time scale of  $\sim 100$  fs  
12  
13 with the target atoms assuming a temperature of 0 K. The extra energy remaining after transferring  
14  
15 the ion kinetic energy ballistically to the target atoms is dissipated by heat conduction to the  
16  
17 surroundings.<sup>53</sup> After the thermalization of the collisions on a time scale of 1-10 ps, thermally  
18  
19 activated processes can cause the generated point defects (vacancy and interstitials) to migrate,  
20  
21 recombine, and create defect complexes on a longer time scale<sup>53</sup> (nanoseconds to years).  
22  
23 Therefore, when comparing the performance of planar and NW solar cells upon irradiation-  
24  
25 induced defects predicted by Monte Carlo BCA simulations, the discrepancies could be due to 1)  
26  
27 the intrinsic limitations of the simulation code to describe the production of point defects in planar  
28  
29 and NWs architectures (*n.b.*, the incapability of modeling the heat spike regime) or 2) other  
30  
31 thermally-activated processes<sup>53,54</sup> with a time scale  $>100$  fs which play a role in transforming and  
32  
33 reducing the residual damage in the NWs relative to that present immediately after the ballistic  
34  
35 collision cascade. Studies of bulk GaAs show that at room temperature the intrinsic defects  
36  
37 (vacancies and interstitials) created during irradiation can interact with previous generated defects  
38  
39 in the crystal<sup>49</sup> which influences the defect migration mechanisms as well as their annihilation and  
40  
41 accumulation. Impurities can promote the creation of stable defect complexes, whereas  
42  
43 dislocations might act as sinks for point defects.<sup>55</sup> Therefore, crystal growth conditions which favor  
44  
45 incorporation of dislocation and other defects or impurities might affect the resulting damage  
46  
47 microstructure as it has been reported particularly in *p*-type GaAs.<sup>49</sup> The planar and the NW solar  
48  
49  
50  
51  
52  
53  
54  
55  
56  
57  
58  
59  
60

1  
2  
3 cells tested are both grown by metallorganic vapor phase epitaxy reactors (MOVPE) but at very  
4  
5 different growth conditions and in different crystal orientations. An excellent crystal quality was  
6  
7 observed in the transmission electron microscopy (TEM) images taken in the NW solar cells tested  
8  
9 (Figures S.4).

10  
11  
12 Finally, it has been widely reported in the literature that the presence of surfaces/interfaces  
13  
14 interact strongly with defects created by collision cascades.<sup>55,56</sup> Interfaces can attract, absorb and  
15  
16 annihilate defects.<sup>57-60</sup> Therefore, nanostructured materials with a high surface-to-volume ratio are  
17  
18 expected to exhibit a radiation damage tolerance significantly different from bulk materials.  
19  
20 Additionally, in the case of NWs, observation of enhanced dynamic annealing and absence of  
21  
22 extended defects due to the dimensional confinement has been reported in Ge<sup>61</sup> and GaN NWs.<sup>62</sup>  
23  
24  
25  
26 Further computational work is required to extend the knowledge of the behavior of the NW arrays  
27  
28 under irradiation and to correlate to the electronic properties observed. In order to achieve accurate  
29  
30 predictions, the NW array needs to be analyzed with tools which are able to model the evolution  
31  
32 of the system from the ballistic collision until the irradiation-induced defects become immobile.<sup>60</sup>

33  
34  
35 While Monte Carlo BCA simulations can only be used to make qualitative predictions; they can  
36  
37 be used to optimize the NW array to increase the radiation hardness. In fact, Monte Carlo BCA  
38  
39 simulations revealed that the damage in free-standing NWs is even lower. An array of free-  
40  
41 standing NWs would behave like a planar device for light absorption but like a hollow structure  
42  
43 for the irradiation with high energy particles.  
44  
45  
46  
47  
48

## 49 CONCLUSION

50  
51  
52 In conclusion, III-V NW array solar cells have the potential to become efficient, lightweight,  
53  
54 radiation-tolerant power-generating devices for space applications. In addition, since III-V NW  
55  
56  
57  
58  
59  
60

1  
2  
3 array solar cells are made of the same semiconductor materials as standard space multijunction  
4 solar cells, they should benefit from the long heritage in development of III-V photovoltaic device  
5 technologies for space applications. Our results also indicate that further increases in radiation-  
6 robustness and specific power can be anticipated for approaches that feature 1) processing of NW  
7 devices infilled with an ultralow density mechanically stable material (such as aerogel) and 2)  
8 developing efficient substrate-free devices, could lead to a breakthrough in the development of  
9 electronic devices for space applications.  
10  
11  
12  
13  
14  
15  
16  
17  
18  
19  
20

## 21 METHODS

22  
23  
24 **Solar cells synthesis and fabrication.** NWs were grown in a horizontal metalorganic vapor phase  
25 epitaxy (MOVPE) reactor with the vapour-liquid-solid method on (111B) substrates with  
26 predefined hexagonal or square array of Au nanodiscs with a pitch of ~500 nm placed by  
27 nanoimprint lithography.<sup>63</sup> For GaAs NW growth, a *p*-type GaAs substrate of  $5 \cdot 10^{17} \text{ cm}^{-3}$  was  
28 employed whereas for InP NW growth a *p*-type InP substrate of  $5 \cdot 10^{18} \text{ cm}^{-3}$  was used. Typical  
29 growth temperatures were around 450 °C, at which the appropriate metalorganics are added to the  
30 carrying gas (H<sub>2</sub>) to grow the linear *n-p* structures. Total lengths are 1.7-2 and 3-3.2 μm for the  
31 InP and GaAs case, respectively. Given the high aspect ratio of the semiconductor structures,  
32 special attention must be given to surface passivation. In particular, GaAs samples included an *in*  
33 *situ* grown AlGaAs passivation shell<sup>31</sup> whereas passivation of InP relied on *ex situ* oxide  
34 deposition.<sup>32</sup> Further details on InP and GaAs NW MOVPE growth can be found in references,<sup>32,31</sup>  
35 respectively.  
36  
37  
38  
39  
40  
41  
42  
43  
44  
45  
46  
47  
48  
49  
50  
51

52 Samples were processed into 1.049 mm<sup>2</sup> solar cells in the case of the GaAs nanowire solar cells  
53 and into 0.86 mm<sup>2</sup> in the case of the InP nanowire devices. Details about the processing can be  
54  
55  
56  
57

1  
2  
3 found elsewhere,<sup>31</sup> but basically it consist of 1) conformal SiO<sub>x</sub> deposition around the wires 2)  
4 planarization of the array by spin-coating CYCLOTENE resin (Dow Chemical), 3) etch back the  
5 Au catalyst particles by selective wet etching to expose the tip of the wires and 4) Indium tin oxide  
6 (ITO) deposition top contact. Due to the small cell area, no current spreading fingers were  
7 necessary in the InP solar cells and a comb-like front grid was defined with a standard  
8 photolithography process in the case of the slightly larger GaAs solar cells. In both cases the  
9 sample back-side was glued with Ag paste to a brass coin, serving as back contact.

10  
11  
12  
13  
14  
15  
16  
17  
18  
19 The planar *n* on *p* GaAs solar cells included in this study were grown inverted on top of a 5 nm  
20 sacrificial layer of Al<sub>0.9</sub>Ga<sub>0.1</sub>As grown on a GaAs substrate. The semiconductor structure was  
21 grown in a MOVPE reactor by Spectrolab and the samples were processed into 8.41 mm<sup>2</sup> thin film  
22 solar cells at Caltech. Extended details about the solar cell processing can be found in <sup>64</sup> but in  
23 brief it comprises the following steps: 1) evaporation of a highly reflective back mirror which will  
24 also serve as the back contact, 2) electroplating a thick copper handle substrate (~50 μm) on top  
25 of the rear mirror, 3) bonding the copper film plated to a silicon wafer with black wax to ease the  
26 handling of the samples, 4) etch the Al<sub>0.9</sub>Ga<sub>0.1</sub>As sacrificial layer by immersing the sample into  
27 HF:C<sub>2</sub>H<sub>6</sub>O (1:1) to lift-off the thin film GaAs solar cell from the thick substrate, 5) standard  
28 photolithography techniques to define the inverted square front grid contact, 6) evaporation of the  
29 front contact which consist of Pd/Ge/Au, 7) metal lift-off, 8) front contact annealing at 200 °C, 9)  
30 contact layer removal and 10) mesa isolation by using a second photolithography step and wet  
31 chemical etching. It has to be noted that anti-reflecting coating (ARC) has not been deposited on  
32 the devices.

33  
34  
35  
36  
37  
38  
39  
40  
41  
42  
43  
44  
45  
46  
47  
48  
49  
50  
51 The planar *n* on *p* InGaP solar cells tested were grown and fabricated by the National Renewable  
52 Energy Laboratory (NREL). The solar cells were grown inverted by atmospheric pressure MOVPE  
53  
54  
55  
56  
57

1  
2  
3 reactor on (001) GaAs substrates miscut  $6^\circ$  toward (111)A as described previously.<sup>65</sup> After growth  
4 the consequent processing steps were followed:<sup>66</sup> 1) electroplate a Au back contact 2) bonding the  
5 samples to Si handles, 3) substrate removal *via* chemical etching, 4) standard photolithography to  
6 define the comb-like front grid, 5) evaporation of the Ni/Au front contact, 5) contact layer removal  
7 by chemical etching, 6) second photolithography step to define the mesa etching areas, 7) wet  
8 chemical etching to isolate the devices by fully etching down the semiconductor till the Au back  
9 contact is exposed. As in the case of the GaAs ELO solar cells ARC was not deposited on the  
10 GaInP devices.  
11  
12  
13  
14  
15  
16  
17  
18  
19  
20  
21  
22  
23

24 **Electron and Proton Radiation Testing.** The proton testing was carried out in The Aerospace  
25 Corporation facilities in vacuum ( $1 \cdot 10^{-6}$  Torr), at room temperature, the proton beam had a normal  
26 incidence on the sample and the proton flux was  $6 \cdot 10^7$  p<sup>+</sup>/cm<sup>2</sup>·s. The electron testing was  
27 performed in Boeing Radiation Effects Laboratory also in vacuum ( $3 \cdot 10^{-7}$  Torr) at 23 °C and under  
28 normal radiation with an electron flux of  $2 \cdot 10^{11}$  e<sup>-</sup>/cm<sup>2</sup>·s.  
29  
30  
31  
32  
33  
34  
35  
36  
37

38 **Solar Cell Performance Characterization.** The solar simulator used in the characterization  
39 before and after the irradiation tests makes use of an AM1.5G filter. In order to characterize and  
40 control the spectrum of the solar simulator Spectrolab XTJ calibrated isotype solar cells for AM0  
41 were used. The isotype top cell of InGaP (350-670 nm) measured  $\sim 0.5$  suns (AM0) and the isotype  
42 middle cell of GaAs (500-950 nm)  $\sim 0.9$  suns (AM0). The solar cells were measured in air at room  
43 temperature.  
44  
45  
46  
47  
48  
49  
50

51 The initial NW solar cells efficiency under AM1.5G of  $\sim 11.6 \% \pm 0.9 \%$  for GaAs NW solar  
52 cells and  $\sim 6.5 \% \pm 0.9 \%$  for InP NWs reported in the Results and Discussion section has been  
53  
54  
55  
56  
57

1  
2  
3 obtained from the measurements in an Oriel Sol1A solar simulator with an AM1.5G filter. A Si  
4  
5 calibrated reference solar cell was used to adjust the power of the lamp and the measurements were  
6  
7 carried out in air at room temperature.  
8  
9

10  
11  
12 **Simulations Monte Carlo BCA.** The evaluation of the damage distribution in the different device  
13  
14 architectures has been carried out with the program iradina.<sup>52</sup> The code simulates the ion transport  
15  
16 through the matter by means of a Monte Carlo algorithm. Similarly to the well-known SRIM code<sup>67</sup>  
17  
18 iradina uses the random phase approximation, the binary collision approximation, the central  
19  
20 potential approximation and treats the target as an amorphous structure with homogeneous mass  
21  
22 density. The main advantage of iradina is the possibility of simulating 3D geometries. The target  
23  
24 structure is defined by a box divided into equally-sized elementary units which account for the  
25  
26 damage produced inside the unit; thus, generating the 3D damage distribution in the defined  
27  
28 geometry. Further details about the physics behind the model and its limitations can be found in  
29  
30 <sup>52</sup>. Here, a volume of 1.5  $\mu\text{m}$  x 1.5  $\mu\text{m}$  x 3  $\mu\text{m}$  subdivided into elementary units of 10 nm x 10 nm  
31  
32 x 20 nm has been simulated. Periodic boundary conditions (PBC) have been assumed laterally to  
33  
34 mimic an infinite array. The front surface (1.5  $\mu\text{m}$  x 1.5  $\mu\text{m}$ ) has been hit with 1,000,000 normal  
35  
36  $\text{H}^+$  of different energies randomly distributed. The displacement threshold energy for Ga and As  
37  
38 has been assumed in all the cases 10 eV.  
39  
40  
41  
42  
43  
44  
45

## 46 47 ACKNOWLEDGMENTS

48  
49  
50 The authors acknowledge financial support from the Space Solar Power Project. The work  
51  
52 performed within NanoLund was supported by the Swedish Research Council (Vetenskapsrådet),  
53  
54 the Swedish Foundation for Strategic Research (SSF), and the Swedish Energy Agency. This  
55  
56  
57

1  
2  
3 research has been funded by Knut and Alice Wallenberg Foundation. This project has received  
4  
5 funding from the European Union's Horizon 2020 research and innovation programme under grant  
6  
7 agreement No 641023 (Nano-Tandem) and under the Marie Skłodowska-Curie grant agreement  
8  
9 No 656208. This publication reflects only the author's views and the funding agency is not  
10  
11 responsible for any use that may be made of the information it contains. We gratefully  
12  
13 acknowledge critical support and infrastructure provided for this work by the Kavli Nanoscience  
14  
15 Institute at Caltech. We acknowledge the helpful contributions of J. Lloyd with the solar cell  
16  
17 processing of the ELO GaAs solar cells at Caltech. We acknowledge The Aerospace Corporation  
18  
19 for the irradiation test with protons and Boeing Radiation Effects Laboratory for the irradiation  
20  
21 with electrons. This work was supported by the U.S. Department of Energy under Contract No.  
22  
23 DE-AC36-08GO28308 with Alliance for Sustainable Energy, LLC, the operator of the National  
24  
25 Renewable Energy Laboratory. This publication reflects only the author's views and not  
26  
27 necessarily the DOE or U.S. government, and the funding agency is not responsible for any use  
28  
29 that may be made of the information it contains. The U.S. Government retains and the publisher,  
30  
31 by accepting the article for publication, acknowledges that the U.S. Government retains a  
32  
33 nonexclusive, paid-up, irrevocable, worldwide license to publish or reproduce the published form  
34  
35 of this work, or allow others to do so, for U.S. Government purposes.  
36  
37  
38  
39  
40  
41  
42  
43  
44

#### 45 ASSOCIATED CONTENT

46  
47

48 **Supporting Information Available:** 1) characteristic parameters of the different solar cell  
49  
50 architectures before and after irradiation tests, 2) empirical correlation of the degradation of planar  
51  
52 and NW GaAs solar cells under the irradiation with protons of 100 keV and 350 keV, 3) cross  
53  
54 sectional sketches of the NW structures simulated with iradina, 4) electronic energy loss  
55  
56  
57

1  
2  
3 distribution under the irradiation with normal incident 100 keV and 350 keV protons and 5) TEM  
4 images of a NW solar cell irradiated with 100 keV protons at a fluence of  $10^{12}$  p<sup>+</sup>/cm<sup>2</sup>. This material  
5 is available free of charge *via* the internet at <http://pubs.acs.org>.  
6  
7  
8  
9  
10

## 11 12 13 AUTHOR INFORMATION

### 14 15 16 **Corresponding Author**

17  
18 \* e-mail: [haa@caltech.edu](mailto:haa@caltech.edu)  
19  
20

### 21 22 **Present Address**

23 # Institute for Energy Technology, Kjeller, NO-2007, Norway  
24  
25  
26  
27

## 28 29 30 REFERENCES

31 (1) Abdelal, G. F.; Abuelfoutouh, N.; Gad, A. H. *Finite Element Analysis for Satellite Structures:*  
32 *Applications to Their Design, Manufacture and Testing*; Springer-Verlag: London, **2013**; pp 11–  
33  
34 47.  
35  
36  
37

38 (2) Anspaugh, B.E. *GaAs Solar Cell Radiation Handbook*; National Aeronautics and Space  
39 Administration, Jet Propulsion Laboratory, California Institute of Technology: Pasadena, CA,  
40  
41 **1996**; pp 4-1 – 4-18.  
42  
43  
44  
45

46 (3) Yamaguchi, M. Radiation Resistance of Compound Semiconductor Solar Cells. *J. Appl.*  
47 *Phys.* **1995**, 78, 1476–1480.  
48  
49  
50

51 (4) Keavney, C. J.; Walters, R. J.; Drevinsky, P. J. Optimizing the Radiation Resistance of InP  
52 Solar Cells: Effect of Dopant Density and Cell Thickness. *J. Appl. Phys.* **1993**, 73, 60–70.  
53  
54  
55  
56  
57



1  
2  
3 (5) Takamoto, T.; Kaneiwa, M.; Imaizumi, M.; Yamaguchi, M. InGaP/GaAs-Based  
4 Multijunction Solar Cells. *Prog. Photovolt: Res. Appl.* **2005**, 13, 495–511.  
5  
6

7  
8 (6) Adams, J. G.; Elarde, V. C.; Hillier, G.; Stender, C.; Tuminello, F.; Wibowo, A.; Youtsey,  
9 C.; Bittner, Z.; Hubbard, S. M.; Clark, E. B.; Piszczor, M. F.; Osowski, M. Improved Radiation  
10 Resistance of Epitaxial Lift-Off Inverted Metamorphic Solar Cells. In *39th IEEE Photovoltaic*  
11 *Specialists Conference*, Tampa, FL, **2013**, 3229–3232.  
12  
13  
14  
15

16  
17 (7) Hubbard, S. M.; Bailey, C.; Polly, S.; Cress, C.; Andersen, J.; Forbes, D.; Raffaele, R.  
18 Nanostructured Photovoltaics for Space Power. *J. Nanophotonics* **2009**, 3, 031880.  
19  
20  
21  
22

23  
24 (8) Law, D. C.; Chiu, P. T.; Fetzer, C. M.; Haddad, M.; Mesropian, S.; Cravens, R.; Hebert, P.  
25 H.; Ermer, J. H.; Krogen, J. P. Development of XTJ Targeted Environment (XTE) Solar Cells for  
26 Specific Space Applications. In *IEEE 7th World Conference on Photovoltaic Energy Conversion*,  
27 Waikoloa Village, HI, **2018**, 3360–3363.  
28  
29  
30  
31

32  
33 (9) Derkacs, D.; Aiken, D.; Bittner, Z.; Cruz, S.; Haas, A.; Hart, J.; McPheeters, C.; Kerestes,  
34 C.; Miller, N.; Patel, P.; Riley, M.; Sharps, P.; Stavrides, A.; Struempel, C.; Whipple, S.  
35 Development of IMM- $\alpha$  and Z4J Radiation Hard III-V Solar Cells. In *IEEE 7th World Conference*  
36 *on Photovoltaic Energy Conversion*, Waikoloa Village, HI, **2018**, 3757–3762.  
37  
38  
39  
40  
41

42  
43 (10) Law, D. C.; Edmondson, K.M.; Siddiqi, N.; Paredes, A.; King, R.R.; Glenn, G.; Labios, E.;  
44 Haddad, M.H.; Isshiki, T.D.; Karam, N.H. Lightweight, Flexible, High-Efficiency III-V  
45 Multijunction Cells. In *IEEE 4th World Conference on Photovoltaic Energy Conference*,  
46 Waikoloa, HI, **2006**, 1879–1882.  
47  
48  
49  
50  
51  
52  
53  
54  
55  
56  
57  
58  
59  
60

1  
2  
3 (11) Kayes, B. M.; Zhang, L.; Twist, R.; Ding, I-K.; Higashi, G. S. Flexible Thin-Film Tandem  
4 Solar Cells with > 30 % Efficiency. *IEEE J. Photovolt.* **2014**, 4, 729–733.  
5  
6

7  
8 (12) Gibb, J. Lightweight Flexible Space Solar Arrays, Past, Present and Future. In *IEEE 7th*  
9 *World Conference on Photovoltaic Energy Conversion*, Waikoloa Village, HI, **2018**, 3530–3534.  
10  
11

12  
13 (13) Granata, J. E.; Sahlstrom, T. D.; Hausgen, P.; Messenger, S. R.; Walters, R. J.; Lorentzen,  
14 J. R.; Liu, S.; Helizon, R. Thin-Film Photovoltaic Proton and Electron Radiation Testing for a  
15 MEO Orbit. In *IEEE 4th World Conference on Photovoltaic Energy Conference*, Waikoloa, HI,  
16 **2006**, 1773–1776.  
17  
18  
19  
20  
21

22  
23 (14) Woodyard, J. R.; Landis, G. A. Radiation Resistance of Thin-Film Solar Cells for Space  
24 Photovoltaic Power. *Sol. Cells* **1991**, 31, 297–329.  
25  
26  
27

28  
29 (15) Lang, F.; Shargaieva, O.; Brus, V. V.; Neitzert, H. C.; Rappich, J.; Nickel, N. H. Influence  
30 of Radiation on the Properties and the Stability of Hybrid Perovskites. *Adv. Mater.* **2018**, 30,  
31 1702905.  
32  
33  
34

35  
36 (16) Miyazawa, Y.; Ikegami, M.; Chen, H-W.; Ohshima, T.; Imaizumi, M.; Hirose, K.;  
37 Miyasaka, T. Tolerance of Perovskite Solar Cell to High-Energy Particle Irradiations in Space  
38 Environment. *iScience* **2018**, 2, 148–155.  
39  
40  
41

42  
43 (17) Huang, J-H.; Kelzenberg, M. D.; Espinet-González, P.; Mann, C.; Walker, D.; Naqavi, A.;  
44 Vaidya, N.; Warmann, E.; Atwater, H. A. Effects of Electron and Proton Radiation on Perovskite  
45 Solar Cells for Space Solar Power Application. In *44th IEEE Photovoltaic Specialists Conference*,  
46 Washington, DC, **2017**, 1248–1252.  
47  
48  
49  
50  
51  
52  
53  
54  
55  
56  
57

1  
2  
3 (18) Kang, S.; Jeong, J.; Cho, S.; Yoon, Y. J.; Park, S.; Lim, S.; Kim, J. Y.; Ko, H. Ultrathin,  
4  
5 Lightweight and Flexible Perovskite Solar Cells with an Excellent Power-Per-Weight  
6  
7 Performance. *J. Mater. Chem. A* **2019**, *7*, 1107–1114.  
8  
9

10  
11 (19) Hirst, L. C.; Yakes, M. K.; Warner, J. H.; Bennett, M. F.; Schmieder, K. J.; Walters, R. J.;  
12  
13 Jenkins, P. P. Intrinsic Radiation Tolerance of Ultra-Thin GaAs Solar Cells. *Appl. Phys. Lett.* **2016**,  
14  
15 109, 033908.  
16  
17

18  
19 (20) Leon, R.; Marcinkevicius, S.; Siegert, J.; Cechavicius, B.; Magness, B.; Taylor, W.; Lobo,  
20  
21 C. Effects of Proton Irradiation on Luminescence Emission and Carrier Dynamics of Self-  
22  
23 Assembled III-V Quantum Dots. *IEEE Trans. Nucl. Sci.* **2002**, *49*, 2844–2851.  
24  
25

26  
27 (21) Marcinkevičius, S.; Siegert, J.; Leon, R.; Čechavičius, B.; Magness, B.; Taylor, W.; Lobo,  
28  
29 C. Changes in Luminescence Intensities and Carrier Dynamics Induced by Proton Irradiation in  
30  
31  $\text{In}_x\text{Ga}_{1-x}\text{As}/\text{GaAs}$  Quantum Dots. *Phys. Rev. B* **2002**, *66*, 235314.  
32  
33

34  
35 (22) Kerestes, C.; Forbes, D.; Bailey, C. G.; Spann, J.; Richards, B.; Sharps, P.; Hubbard, S.  
36  
37 Radiation Effects on Quantum Dot Enhanced Solar Cells. *Proc. SPIE 8256, Physics, Simulation,*  
38  
39 *and Photonic Engineering of Photovoltaic Devices* **2012**, 82561I.  
40  
41

42  
43 (23) Bailey, C. G.; Hoheisel, R.; Gonzalez, M.; Forbes, D. V.; Lumb, M. P.; Hubbard, S. M.;  
44  
45 Scheiman, D. A.; Hirst, L. C.; Schmieder, K.; Messenger, S.; Weaver, B.; Cress, C. D.; Warner,  
46  
47 J.; Yakes, M. K.; Jenkins, P. P.; Walters, R. J. Radiation Effects on InAlGaAs/InGaAs Quantum  
48  
49 Well Solar Cells. In *40th IEEE Photovoltaic Specialists Conference*, Denver, CO, **2014**, 2871–  
50  
51 2874.  
52  
53  
54  
55  
56  
57  
58  
59  
60

1  
2  
3 (24) Anttu, N.; Xu, H. Q. Efficient Light Management in Vertical Nanowire Arrays for  
4 Photovoltaics. *Opt. Express* **2013**, 21, A558–A575.

5  
6  
7  
8 (25) Garnett, E. C.; Brongersma, M. L.; Cui, Y.; McGehee, M. D. Nanowire Solar Cells. *Annu.*  
9  
10  
11 *Rev. Mater. Res.* **2011**, 41, 269–295.

12  
13 (26) LaPierre, R. R.; Chia, A. C. E.; Gibson, S. J.; Haapamaki, C. M.; Boulanger, J.; Yee, R.;  
14  
15  
16  
17  
18 Kuyanov, P.; Zhang, J.; Tajik, N.; Jewell, N.; Rahman, K. M. A. III-V Nanowire Photovoltaics:  
19  
20  
21 Review of Design for High Efficiency. *Phys. Status Solidi RRL* **2013**, 7, 815–830.

22 (27) Barrigón, E.; Heurlin, M.; Bi, Z.; Monemar, B.; Samuelson, L. Synthesis and Applications  
23  
24  
25 of III-V Nanowires. *Chem. Rev.* **2019**, 119, 9170–9220.

26  
27 (28) Tan, L-Y.; Li, F-J.; Xie, X-L.; Zhou, Y-P.; Ma, J. Proton Radiation Effect on GaAs/AlGaAs  
28  
29  
30 Core-Shell Ensemble Nanowires Photo-Detector. *Chin. Phys. B* **2017**, 26, 086202.

31  
32 (29) Tan, L-Y.; Li, F-J.; Xie, X-L.; Zhou, Y-P.; Ma, J. Study on Irradiation-Induced Defects in  
33  
34  
35  
36  
37 GaAs/AlGaAs Core–Shell Nanowires *via* Photoluminescence Technique. *Chin. Phys. B* **2017**, 26,  
38  
39 086201.

40 (30) Li, F.; Li, Z.; Tan, L.; Zhou, Y.; Ma, J.; Lysevych, M.; Fu, L.; Tan H. H.; Jagadish, C.  
41  
42  
43  
44  
45 Radiation Effects on GaAs/AlGaAs Core/Shell Ensemble Nanowires and Nanowire Infrared  
46  
47 Photodetectors. *Nanotechnology* **2017**, 28, 125702.

48 (31) Åberg, I.; Vescovi, G.; Asoli, D.; Naseem, U.; Gilboy, J. P.; Sundvall, C.; Dahlgren, A.;  
49  
50  
51  
52  
53 Svensson, K. E.; Anttu, N.; Björk, M. T.; Samuelson L. A GaAs Nanowire Array Solar Cell with  
54  
55  
56  
57  
58 15.3 % Efficiency at 1 Sun. *IEEE J. Photovolt.* **2016**, 6, 185–190.

1  
2  
3 (32) Otnes, G.; Barrigón, E.; Sundvall, C.; Svensson, K. E.; Heurlin, M.; Siefer, G.; Samuelson,  
4 L.; Åberg, I.; Borgström, M. T. Understanding InP Nanowire Array Solar Cell Performance by  
5 Nanoprobe-Enabled Single Nanowire Measurements. *Nano Lett.* **2018**, 18, 3038–3046.  
6  
7

8  
9  
10 (33) van Dam, D.; van Hoof, N. J. J.; Cui, Y.; van Veldhoven, P. J.; Bakkers, E. P. A. M.; Rivas,  
11 J. G.; Haverkort, J. E. M. High-Efficiency Nanowire Solar Cells with Omnidirectionally Enhanced  
12 Absorption Due to Self-Aligned Indium-Tin-Oxide Mie Scatterers. *ACS Nano* **2016**, 10, 11414–  
13 11419.  
14  
15  
16  
17  
18

19  
20 (34) Chen, Y.; Pistol, M-E.; Anttu, N. Design for Strong Absorption in a Nanowire Array  
21 Tandem Solar Cell. *Sci. Rep.* **2016**, 6, 32349.  
22  
23  
24  
25

26 (35) Gudiksen, M. S.; Lauhon, L. J.; Wang, J.; Smith, D. C.; Lieber, C. M. Growth of Nanowire  
27 Superlattice Structures for Nanoscale Photonics and Electronics. *Nature* **2002**, 415, 617–620.  
28  
29  
30

31 (36) Björk, M. T.; Ohlsson, B. J.; Sass, T.; Persson, A. I.; Thelander, C.; Magnusson, M. H.;  
32 Deppert, K.; Wallenberg, L. R.; Samuelson, L. One-Dimensional Steeplechase for Electrons  
33 Realized. *Nano Lett.* **2002**, 2, 87–89.  
34  
35  
36  
37  
38

39 (37) Mårtensson, T.; Svensson, C. P. T.; Wacaser, B. A.; Larsson, M. W.; Seifert, W.; Deppert,  
40 K.; Gustafsson, A.; Wallenberg, L. R.; Samuelson, L. Epitaxial III-V Nanowires on Silicon. *Nano*  
41 *Lett.* **2004**, 4, 1987–1990.  
42  
43  
44  
45

46 (38) Bakkers, E. P. A. M.; van Dam, J. A.; De Franceschi, S.; Kouwenhoven, L. P.; Kaiser, M.;  
47 Verheijen, M.; Wondergem, H.; van der Sluis, P. Epitaxial Growth of InP Nanowires on  
48 Germanium. *Nat. Mater.* **2004**, 3, 769–773.  
49  
50  
51  
52  
53  
54  
55  
56  
57  
58  
59  
60

1  
2  
3 (39) Heurlin, M.; Magnusson, M.; Lindgren, D.; Wallenberg, R.; Deppert, K.; Samuelson, L.  
4  
5 Continuous Gas-Phase Synthesis of Nanowires with Tunable Properties. *Nature* **2012**, 492, 90–  
6  
7 94.

8  
9  
10 (40) Barrigón, E.; Hultin, O.; Lindgren, D.; Yadegari, F.; Magnusson, M.; Samuelson, L.;  
11  
12 Johansson, L.; Björk, M. GaAs Nanowire *PN*-Junctions Produced by Low-Cost and High-  
13  
14 Throughput Aerotaxy. *Nano Lett.* **2018**, 18, 1088–1092.

15  
16 (41) Borgström, M.; Magnusson, M.; Dimroth, F.; Siefert, G.; Höhn, O.; Riel, H.; Schmid, H.;  
17  
18 Wirths, S.; Björk, M.; Åberg, I.; Peijnenburg, W.; Vijver, M.; Tchernycheva, M.; Piazza, V.;  
19  
20 Samuelson, L. Towards Nanowire Tandem Junction Solar Cells on Silicon. *IEEE J. Photovolt.*  
21  
22 **2018**, 8, 733–740.

23  
24 (42) Standing, A. J.; Assali, S.; Haverkort, J. E. M.; Bakkers, E. P. A. M. High Yield Transfer  
25  
26 of Ordered Nanowire Arrays into Transparent Flexible Polymer Films. *Nanotechnology* **2012**, 23,  
27  
28 495305.

29  
30 (43) Fan, Z.; Razavi, H.; Do, J-W.; Moriwaki, A.; Ergen, O.; Chueh, Y-L.; Leu, P.W.; Ho, J.C.;  
31  
32 Takahashi, T.; Reichertz, L.A.; Neale, S.; Yu, K.; Wu, M.; Ager, J. W.; Javey, A. Three-  
33  
34 Dimensional Nanopillar-Array Photovoltaics on Low-Cost and Flexible Substrates. *Nat. Mater.*  
35  
36 **2009**, 8, 648–653.

37  
38 (44) Dai, X.; Messanvi, A.; Zhang, H.; Durand, C.; Eymery, J.; Bougerol, C.; Julien, F. H.;  
39  
40 Tchernycheva, M. Flexible Light-Emitting Diodes Based on Vertical Nitride Nanowires. *Nano*  
41  
42 *Lett.* **2015**, 15, 6958–6964.  
43  
44  
45  
46  
47  
48  
49  
50  
51  
52  
53  
54  
55  
56  
57  
58  
59  
60

1  
2  
3 (45) Fountaine, K. T.; Cheng, W-H.; Bukowsky, C. R.; Atwater, H. A. Near-Unity Unselective  
4 Absorption in Sparse InP Nanowire Arrays. *ACS Photonics* **2016**, 3, 1826–1832.

7  
8 (46) Tada, H. Y.; Carter, J. R.; Anspaugh, B. E.; Downing, R. G. *Solar Cell Radiation Handbook*;  
9 National Aeronautics and Space Administration, Jet Propulsion Laboratory, California Institute of  
10 Technology: Pasadena, CA, **1982**; pp 3-1 – 3-153.

13  
14 (47) Anspaugh, B. E. Proton and Electron Damage Coefficients for GaAs/Ge Solar Cells. In  
15  
16  
17  
18  
19  
20  
21  
22  
23  
24  
25  
26  
27  
28  
29  
30  
31  
32  
33  
34  
35  
36  
37  
38  
39  
40  
41  
42  
43  
44  
45  
46  
47  
48  
49  
50  
51  
52  
53  
54  
55  
56  
57  
58  
59  
60  
*22nd IEEE Photovoltaic Specialists Conference*, Las Vegas, NV, **1991**, 1593–1598.

(48) Warner, J. H.; Messenger, S. R.; Walters, R. J.; Summers, G. P.; Lorentzen, J. R.; Wilt, D.  
M.; Smith, M. A. Correlation of Electron Radiation Induced-Damage in GaAs Solar Cells. *IEEE  
Trans. Nucl. Sci.* **2006**, 53, 1988–1994.

(49) Pons, D.; Bourgoin, J. C. Irradiation-Induced Defects in GaAs. *J. Phys. C: Solid State Phys.*  
**1985**, 18, 3839–3871.

(50) Chen, Y.; Kivisaari, P.; Pistol, M. E.; Anttu, N. Optimized Efficiency in InP Nanowire Solar  
Cells with Accurate 1D Analysis. *Nanotechnology* **2018**, 29, 045401.

(51) Sharps, P. R.; Aiken, D. J.; Stan, M. A.; Thang, C. H.; Fatemi, N. Proton and Electron  
Radiation Data and Analysis of GaInP<sub>2</sub>/GaAs/Ge Solar Cells. *Prog. Photovoltaics: Res. Appl.*  
**2002**, 10, 383–390.

(52) Borschel, C.; Ronning, C. Ion Beam Irradiation of Nanostructures – A 3D Monte Carlo  
Simulation Code. *Nucl. Instrum. Methods Phys. Res. Sect. B* **2011**, 269, 2133–2138.

(53) Nordlund, K.; Djurabekova, F. Multiscale Modelling of Irradiation in Nanostructures. *J.  
Comput. Electron.* **2014**, 13, 122–141.

1  
2  
3 (54) Krasheninnikov, A. V.; Nordlund, K. Ion and Electron Irradiation-Induced Effects in  
4 Nanostructured Materials. *J. Appl. Phys.* **2010**, 107, 071301.

5  
6  
7  
8 (55) Doan, N. V.; Martin, G. Elimination of Irradiation Point Defects in Crystalline Solids: Sink  
9 Strengths. *Phys. Rev. B* **2003**, 67, 134107.

10  
11  
12  
13 (56) Kelly, R. A.; Holmes, J. D.; Petkov, N. Visualising Discrete Structural Transformations in  
14 Germanium Nanowires During Ion Beam Irradiation and Subsequent Annealing. *Nanoscale* **2014**,  
15 6, 12890–12897

16  
17  
18 (57) Han, W.; Demkowicz, M. J.; Mara, N. A.; Fu, E.; Sinha, S.; Rollett, A. D.; Wang, Y.;  
19 Carpenter, J. S.; Beyerlein, I. J.; Misra, A. Design of Radiation Tolerant Materials *via* Interface  
20 Engineering. *Adv. Mater.* **2013**, 25, 6975–6979.

21  
22 (58) Beyerlein, I. J.; Demkowicz, M. J.; Misra, A.; Uberuaga, B. P. Defect-Interface Interactions.  
23 *Prog. Mater. Sci.* **2015**, 74, 125–210.

24  
25 (59) Beyerlein, I. J.; Caro, A.; Demkowicz, M. J.; Mara, N. A.; Misra, A.; Uberuaga, B.P.  
26 Radiation Damage Tolerant Nanomaterials. *Mater. Today* **2013**, 16, 443–449.

27  
28 (60) Bai, X-M.; Voter, A. F.; Hoagland, R. G.; Nastasi, M.; Uberuaga, B. P. Efficient Annealing  
29 of Radiation Damage Near Grain Boundaries *via* Interstitial Emission. *Science* **2010**, 327, 1631–  
30 1634.

31  
32 (61) Koleśnik-Gray, M. M.; Sorger, C.; Biswas, S.; Holmes, J. D.; Weber, H. B.; Krstić, V. In  
33 Operandi Observation of Dynamic Annealing: A Case Study of Boron in Germanium Nanowire  
34 Devices. *Appl. Phys. Lett.* **2015**, 106, 233109.



1  
2  
3 (62) Dhara, S.; Datta, A.; Wu, C. T.; Lan, Z. H.; Chen, K. H.; Wang, Y. L. Enhanced Dynamic  
4 Annealing in Ga<sup>+</sup> Ion-Implanted GaN Nanowires. *Appl. Phys. Lett.* **2003**, 82, 451–453.  
5  
6

7  
8 (63) Otnes, G.; Heurlin, M.; Graczyk, M.; Wallentin, J.; Jacobsson, D.; Berg, A.; Maximov, I.;  
9 Borgström, M. T. Strategies to Obtain Pattern Fidelity in Nanowire Growth from Large-Area  
10 Surfaces Patterned Using Nanoimprint Lithography. *Nano Res.* **2016**, 9, 2852–2861.  
11  
12  
13

14  
15 (64) Lloyd, J. V. *Optoelectronic Design and Prototyping of Spectrum-Splitting Photovoltaics*;  
16 (Ph.D. Dissertation) California Institute of Technology: Pasadena, CA, **2018**; pp 48–69.  
17  
18  
19

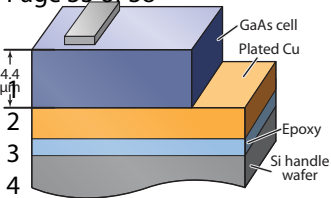
20  
21 (65) Geisz, J. F.; Kurtz, S.; Wanlass, M. W.; Ward, J. S.; Duda, V.; Friedman, D. J.; Olson, J.  
22 M.; McMahon, W. E.; Moriarty, T. E.; Kiehl, J. T. High-Efficiency GaInP/GaAs/InGaAs Triple-  
23 Junction Solar Cells Grown Inverted with a Metamorphic Bottom Junction. *Appl. Phys. Lett.* **2007**,  
24 91, 023502.  
25  
26  
27  
28  
29

30  
31 (66) Duda, A.; Ward, S.; Young, M. *Inverted Metamorphic Multijunction (IMM) Cell Processing*  
32 *Instructions*; National Renewable Energy Laboratory, U.S. Dept. of Energy: Golden, CO, **2012**.  
33  
34  
35

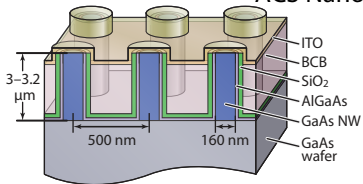
36  
37 (67) Ziegler, J. F.; Ziegler, M. D.; Biersack, J. P. SRIM – The Stopping and Range of Ions in  
38 Matter (2010). *Nucl. Instrum. Methods Phys. Res., Sect. B* **2010**, 268, 1818–1823.  
39  
40  
41  
42  
43  
44  
45  
46  
47  
48  
49  
50  
51  
52  
53  
54  
55  
56  
57  
58  
59  
60

**a** GaAs Planar (ELO)

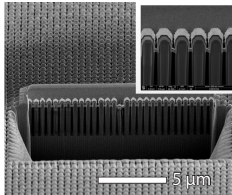
Page 33 of 38



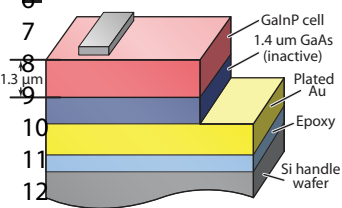
**b** GaAs NW ACS Nano



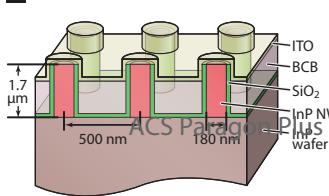
**c** GaAs NW



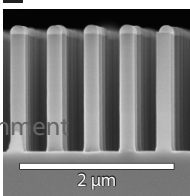
**d** InGaP Planar (ELO)



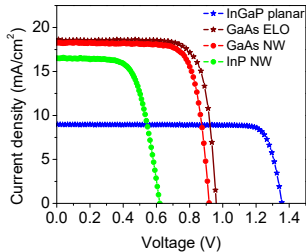
**e** InP NW



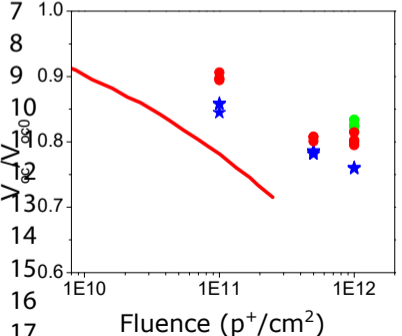
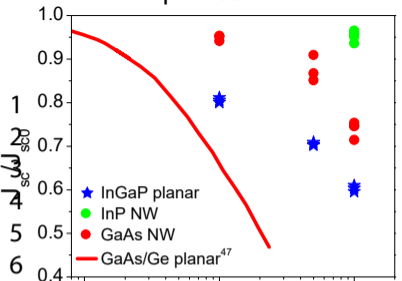
**f** InP NW



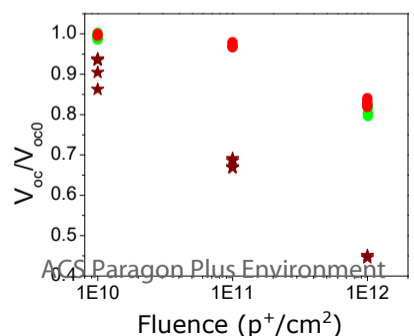
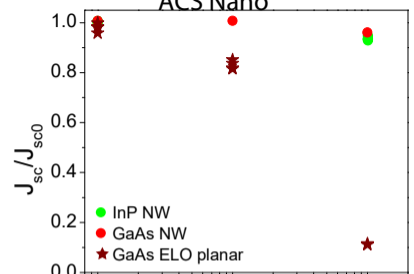
**g** Pre-Radiation *J-V*



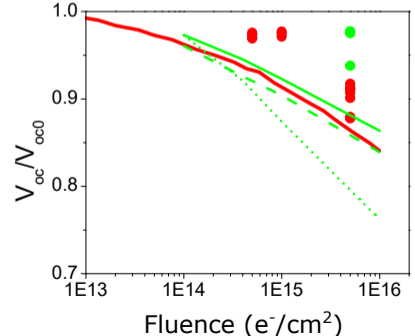
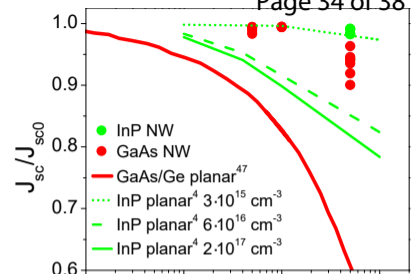
p<sup>+</sup> 100 keV



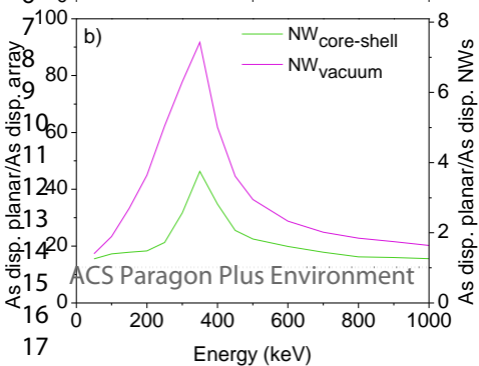
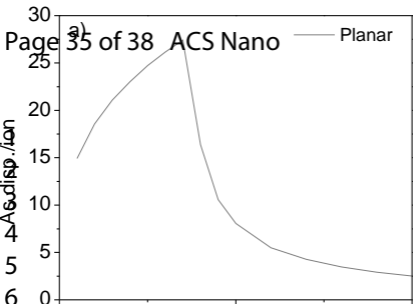
p<sup>+</sup> 350 keV  
ACS Nano



e<sup>-</sup> 1 MeV



ACS Paragon Plus Environment



# Planar

p<sup>+</sup>

# Core-Shell

ACS plano

# Vacuum

p<sup>+</sup>

- GaAs
- AlGaAs
- SiO<sub>2</sub>
- BCB
- Vacuum

